Sneutrino Dark Matter: Symmetry Protection and Cosmic Ray Anomalies

Durmuş A. Demir[a], Lisa L. Everett[b], Mariana Frank[c], Levent Selbuz[a,d], and Ismail Turan[c,e]

[a]*Department of Physics, Izmir Institute of Technology, IZTECH, TR35430 Izmir, Turkey,*
[b]*Department of Physics, University of Wisconsin, Madison, WI53706, USA,*
[c]*Department of Physics, Concordia University, 7141 Sherbrooke St. West, Montreal, Quebec, Canada H4B 1R6,*
[d]*Department of Engineering Physics, Ankara University, TR06100 Ankara, Turkey, and*
[e]*Ottawa-Carleton Institute of Physics, Carleton University,*
1125 Colonel By Drive Ottawa, Ontario, Canada, K1S 5B6.
(Dated: October 31, 2018)

We present an R-parity conserving model of sneutrino dark matter within a Higgs-philic $U(1)'$ extension of the minimal supersymmetric standard model. In this theory, the μ parameter and light Dirac neutrino masses are generated naturally upon the breaking of the $U(1)'$ gauge symmetry. One of the right-handed senutrinos is the LSP. The leptonic and hadronic decays of another sneutrino, taken to be the next-to-lightest superpartner, allow for a natural fit to the recent results reported by the PAMELA experiment. We perform a detailed calculation of the dark matter relic density in this scenario, and show that the model is consistent with the ATIC and FERMI-LAT experiments.

I. INTRODUCTION AND MOTIVATION

The question of the nature of dark matter (DM), which forms nearly one-fourth of the total mass in the universe, is a pivotal question for cosmology, astrophysics, and particle physics. Other than its relic density [1], little is known about the structure of DM. Recently, there has been great excitement that new information about DM may be revealed by the results from the PAMELA satellite [2] claiming an increase in positron fraction in cosmic rays with energies above 10 GeV. Others, including the PPB-BETS [3] and HESS [4] experiments, also claim enhancements in electron/positron flux for energies above 100 GeV. More recently, the FERMI collaboration released a measurement of the e^+e^- flux in the 20 GeV to 1 TeV range [5]. All of these experiments are consistent with a new primary source contributing to local electron/positron fluxes in the $10 - 1000$ GeV range [6]. These anomalies in cosmic ray fluxes may well originate from astrophysical sources such as pulsars or nearby supernova remnants [7]. However, they might also result from the presence of DM particles, providing a golden opportunity to learn more about the properties of DM.

This intriguing possibility has led to a number of proposals that interpret the data as arising from dark matter annihilation [8] (which necessitates an $\mathcal{O}(100)$ boost factor) or decays [9] (which must proceed much slower than the present value of the Hubble parameter). Moreover, PAMELA, while reporting an excess in the electron/positron flux, claims no excess in the proton/antiproton flux [10]. Thus, one intriguing idea is that the DM carries lepton number, *e.g.*, it is composed of right-handed scalar neutrinos (sneutrinos) in minimal [11–13] and extended [14–16] supersymmetric models. This framework might explain the preference for leptonic annihilation/decay products [17–23].

In the simplest extensions of the minimal supersymmetric model (MSSM) that include right-handed neutri-nos, the right-handed neutrinos are gauge singlets. Hence the strength of their Yukawa interactions with the standard model (SM) fields governs whether they thermalize together with the rest of the MSSM matter [12, 14, 18]. On the other hand, if the lightest sneutrino $\widetilde{\nu}_R^1$ is the lightest supersymmetric particle (LSP) and therefore is a potentially viable DM candidate, it can be produced with the right relic density from the decays of heavier superpartners [11]. If the heavier right-handed scalar neutrino $\widetilde{\nu}_R^2$ is the next-to-lightest superpartner (NLSP), its lifetime turns out to be longer than the age of the universe [11, 13]. Therefore, decays of $\widetilde{\nu}_R^2$ should still be active, resulting in observable effects like the excess energetic electrons/positrons in cosmic rays. In the MSSM with right-handed neutrinos, these features have been analyzed with respect to the observed cosmic ray anomalies [23]. However, such right-handed sneutrino dark matter scenarios generically suffer from two aesthetic problems: *(i)* the origin of the suppressed Dirac neutrino Yukawa couplings (though such small couplings are allowed on the basis of technical naturalness [11, 13, 23]), and *(ii)* the origin of the supersymmetric μ parameter [24]. In this paper, we present a $U(1)'$-extended MSSM model in which these aesthetic problems are remedied, and the desirable features of sneutrino DM, including the ability to account for the PAMELA positron excess, can be correctly produced.

II. THE HIGGSPHILIC $U(1)'$-EXTENDED MSSM

It is well known that the MSSM suffers from a naturalness problem due to the presence of the superpotential bilinear operator $\mu \widehat{H}_u \cdot \widehat{H}_d$ [24]. Though the mass parameter μ enters from the superpotential, it must be of the order of the mass terms associated with the supersymmetry breaking sector. This puzzle can be remedied by extending the matter and gauge structure of the MSSM,

e.g. within unified and/or string models [25]. To this end, theories with an extra $U(1)'$ broken at the electroweak-to- TeV scale by SM singlets are known to be able to generate an appropriately sized μ parameter (see *e.g.* [26]).

The $U(1)'$ symmetry can also play a crucial role in generating neutrino masses. The right-handed neutrino sector and the μ parameter can be correlated for both Majorana [27] and Dirac masses [28]. We assume here that lepton number is an accidental symmetry that is conserved at the perturbative level. Hence, the neutrinos are Dirac fermions, requiring Yukawa couplings of $\mathcal{O}\left(10^{-13}\right)$. These couplings are technically natural, but an explanation for such a strong suppression is clearly desirable. One way this can occur is if the $U(1)'$ invariance suppresses leading order contributions to Dirac neutrino masses and allows higher-dimensional operators [28].

In this work, we assume that the $U(1)'$ charges satisfy $Q'_{H_u}+Q'_{H_d} \neq 0$ to forbid the bare μ term, and $Q'_{H_u}+Q'_L+Q'_N \neq 0$ to forbid a bare neutrino Yukawa coupling. After including an SM-singlet chiral superfield $\widehat{S}$, the relevant part of the superpotential takes the form [26, 28]

$$\widehat{W} = h_\mu \widehat{S}\widehat{H}_u \cdot \widehat{H}_d + \frac{1}{M_R}\widehat{S}\widehat{L} \cdot \widehat{H}_u \mathbf{Y}_\nu \widehat{N} \qquad (1)$$

in which the $U(1)'$ invariance requires $Q'_{H_u}+Q'_{H_d}+Q'_S = 0$ and $Q'_{H_u} + Q'_L + Q'_N + Q'_S = 0$. In the above, M_R is a large mass scale, and h_μ and $\mathbf{Y}_\nu$ are the Yukawa couplings responsible for generating the μ parameter and neutrino masses. Upon the breaking of the electroweak and $U(1)'$ gauge symmetries, the effective low energy parameters include the μ parameter

$$\mu = h_\mu \langle S \rangle, \qquad (2)$$

and Dirac neutrino masses

$$\mathbf{m}_\nu = \frac{1}{M_R}\langle S \rangle \langle H_u^0 \rangle \mathbf{Y}_\nu \equiv \overline{\mathbf{Y}}_\nu \left(\langle H_u^0 \rangle / \sin\beta\right). \qquad (3)$$

The effective neutrino Yukawa coupling $\overline{\mathbf{Y}}_\nu$ leads to neutrino masses in good agreement with experiment:

$$\left|\overline{\mathbf{Y}}_\nu\right| \simeq 3 \times 10^{-13} \left(\frac{m_\nu^2}{2.8 \times 10^{-3} \text{ eV}^2}\right)^{1/2}, \qquad (4)$$

for $|\mathbf{Y}_\nu| \sim 1$, $\tan\beta \equiv \langle H_u^0 \rangle / \langle H_d^0 \rangle \sim 1$, and

$$\langle S \rangle \simeq 3 \text{ TeV}, \ M_R \simeq M_{GUT} = 10^{16} \text{ GeV}. \qquad (5)$$

Hence, in this framework the μ problem is resolved and appropriately suppressed Dirac neutrino masses are generated upon $U(1)'$ breaking. Parameter values were chosen to obtain neutrino masses which are in the right range. In the next sections, we give more details of the spectrum constrained by the experimental data.

III. COSMIC RAY ANOMALIES

To account for the anomalous cosmic ray fluxes, there arise several additional constraints on the model. First,

we assume the right-handed neutrino superfields are *total gauge singlets* to avoid unacceptably fast decays that would otherwise occur via gaugino mediated processes. Second, the $U(1)'$ charges must be assigned such that the successful generation of the μ parameter and neutrino masses are maintained. The option that we pursue in this work is to have a "Higgs-philic" $U(1)'$, similar in spirit to [22].

Enforcing these constraints leads to the charge assignments displayed in Table I. Note that of the MSSM fields, only the right-handed up quarks $\widehat{U}$ and the Higgs fields $\widehat{H}_u$ and $\widehat{S}$ have nonvanishing $U(1)'$ charges. The charge assignment in Table I is anomalous as it stands. However, all gauge and gravitational anomalies can be cancelled either by invoking family-dependent $U(1)'$ charges as in [29] (though in this case one needs to worry about constraints from flavor violation), or by augmenting the matter content of the theory by sets of vector-like quark and lepton fields, as well as additional SM singlets that are charged under the $U(1)'$ gauge symmetry. The details will be addressed somewhere else in our future studies.

With this charge assignment, scattering processes that involve $\widehat{H}_u$, $\widehat{S}$ and $\widehat{U}$ are influenced by the $U(1)'$ gauge boson (Z'_μ) and the $U(1)'$ gaugino $(\widetilde{Z}')$ [30]. At hadron colliders, the right-handed up-type quarks $(u_R$ and $c_R)$ can undergo Drell-Yan annihilation through Z'_μ to produce Higgs fields. The decays of the up-type squarks also exhibit novel branchings due to $\widetilde{Z}'$ exchange [30].

Field	$SU(3)_C$	$SU(2)_L$	$U(1)_Y$	$U(1)'$
$\widehat{Q}$	3	2	1/6	0
$\widehat{U}$	$\overline{3}$	1	$-2/3$	$-Q'_{H_u}$
$\widehat{D}$	$\overline{3}$	1	1/3	0
$\widehat{L}$	1	2	$-1/2$	0
$\widehat{N}$	1	1	0	0
$\widehat{E}$	1	1	1	0
$\widehat{H}_u$	1	2	1/2	Q'_{H_u}
$\widehat{H}_d$	1	2	$-1/2$	0
$\widehat{S}$	1	1	0	$-Q'_{H_u}$

TABLE I: *The quantum numbers of quark $(\widehat{Q}, \widehat{U}, \widehat{D})$, lepton $(\widehat{L}, \widehat{N}, \widehat{E})$, and Higgs $(\widehat{H}_u, \widehat{H}_d, \widehat{S})$ superfields. The superpotential couplings of quarks and charged leptons are kept as in the MSSM.*

We now explore the possibility that the excess positron flux observed in the cosmic ray data is due to the presence of sneutrino DM. To do so, we will assume that the soft supersymmetry breaking sector of the theory is such that the lightest right-handed sneutrino $\widetilde{\nu}_R^1$ is the LSP and the next-to-lightest right-handed sneutrino $\widetilde{\nu}_R^2$ is the NLSP.

More explicitly,

$$m_{\widetilde{\nu}_R^1} < m_{\widetilde{\nu}_R^2} < m_{\widetilde{rest}} \qquad (6)$$

where $m_{\widetilde{rest}}$ denotes the remaining superpartner masses, including the heaviest right-handed sneutrino, $\widetilde{\nu}_R^3$. The third heavy particle, the NNLSP, is chosen to be the lightest neutralino, $\widetilde{\chi}_1^0$ and it requires special attention since it decays late enough to have some non-thermal contribution to the DM relic density. The hadronic Big Bang Nucleosynthesis (BBN) constraints will also be considered for the late decaying particles in the model. We discuss these issues further in the next section.

A. The DM relic density

For the spectrum considered above, the DM has two components, the stable LSP and the practically stable NLSP which lives longer than the age of the universe. Together, their relic density should reproduce the WMAP [1] result. The right-handed sneutrino population forms during the cosmic evolution from the decays of the MSSM spectrum plus exotics, which, with a few exceptions, should already have reached thermal equilibrium. A given sparticle decays into right-handed sneutrinos with a rate $\Gamma \sim \left|\overline{\mathbf{Y}}_\nu\right|^2 \times$ (sparticle mass). Therefore, the conversion rate into right-handed sneutrinos is quadratic in the effective neutrino Yukawa coupling $\overline{\mathbf{Y}}_\nu$, and the growth of the LSP number density is fast enough to produce the observed DM relic density [11].

We expect the third sneutrino to also decay to the LSP at freeze-out and thus contribute to the relic density. However, in our chosen parameter space, this sneutrino is taken very heavy (quantified below), much heavier than other sparticles. It would likely mix more with the left-handed sneutrino and decay very quickly compared to the NLSP. Our detailed analysis shows that its life-time ($\sim 10^{-5}$ sec) is larger than its freeze-out time ($\sim 10^{-10}$ sec) but its non-thermal contribution to the relic density is negligible since the branching ratio for decaying into LSP or NLSP is suppressed (less than 10^{-26}).

The right-handed sneutrinos exhibit a non-thermal distribution. To see this, recall that the right-handed sneutrinos mix with the left-handed sneutrinos and therefore interact with the gauge sector. For right-handed sneutrino annihilation, only a four-point interaction, a left-handed sneutrino, or a Higgsino exchange can contribute. The annihilation is out of equilibrium as long as the interaction rate is smaller than the expansion rate $h \sim T^2/M_{Pl}$. The rate of the four-point interaction $\Gamma_4 \sim \left|\overline{\mathbf{Y}}_\nu\right|^4 T < h$, since $\left|\overline{\mathbf{Y}}_\nu\right| \sim 10^{-13}$. The left-handed sneutrino and Higgsino exchanges also have rates $\Gamma_{\widetilde{\nu}_L}$, $\Gamma_{\widetilde{H}_u} < h$, and hence the right-handed sneutrinos do not thermalize before the electroweak phase transition. This is maintained after the phase transition if the mixing with the active (left-handed) sneutrino is small [11, 31].

For a detailed calculation of the relic density, the model must be considered in detail and all the mixings, masses and branching ratios must be determined so that we would calculate the relic density by counting all possible channels. Moreover, we need to evaluate the would-be relic density of the late decaying NNLSP which is computed with through conventional methods. We implement the model fully into the CalcHEP [32] package program with the help of LanHEP [33] program. Once the CalcHEP model files are provided, we use the MicrOMEGAs [34] software for calculating the NNLSP relic density.

In the implementation, we consider a normal hierarchy for the neutrinos and chose the mixing parameters to be $\sin^2 2\theta_{12} = 0.87$, $\sin^2 2\theta_{23} = 0.92$, and $\sin^2 2\theta_{13} = 0.02$. The parametrization of the mixing matrix is identical to the one in the quark sector and the additional CP-violating phases are taken zero. As the positron excess is proportional to the neutrino masses, we keep these non-zero, consistent with the following constraints: $\Delta m_{21}^2 = (7.59 \pm 0.20) \times 10^{-5} \text{eV}^2$ and $\Delta m_{32}^2 = (2.43 \pm 0.13) \times 10^{-3} \text{eV}^2$ [35]. We take M_R, μ, $\tan\beta$, and h_μ as free parameters and express $\langle S \rangle$, $\mathbf{Y}_\nu$ and $\overline{\mathbf{Y}}_\nu$ in terms of them.

In this model the sneutrinos also mix, and the mixing matrix can in general be expressed as

$$\mathcal{L}_m^{\widetilde{\nu}} = -\sum_{i,j=1}^3 (\widetilde{\nu}_L^{i*} \widetilde{\nu}_R^{j*}) \begin{pmatrix} m_{\widetilde{\nu}_{LL}}^2 & m_{\widetilde{\nu}_{LR}}^{2\,ij} \\ m_{\widetilde{\nu}_{RL}}^{2\,ij} & m_{\widetilde{\nu}_{RR}}^{2\,j} \end{pmatrix} \begin{pmatrix} \widetilde{\nu}_L^i \\ \widetilde{\nu}_R^j \end{pmatrix}, \quad (7)$$

where i, j are the flavor indices and the matrix elements are given by

$$\begin{aligned} m_{\widetilde{\nu}_{LL}^i}^2 &= \tfrac{1}{4}g^2(\langle H_d^0\rangle^2 - \langle H_u^0\rangle^2) + g_Y^2(\langle H_d^0\rangle^2 Y_{H_d}Y_L \\ &\quad + \langle H_u^0\rangle^2 Y_{H_u}Y_L) + g_{Y'}^2(\langle H_d^0\rangle^2 Q'_{H_d}Q'_L \\ &\quad + \langle H_u^0\rangle^2 Q'_{H_u}Q'_L + \langle S\rangle^2 Q'_L Q'_S) \\ &\quad + (\mathbf{m}_\nu^{ii})^2 + M_{L_i}^2 \\ m_{\widetilde{\nu}_{RR}^j}^2 &= g_Y^2(\langle H_d^0\rangle^2 Y_{H_d}Y_N + \langle H_u^0\rangle^2 Y_{H_u}Y_N) \\ &\quad + g_{Y'}^2(\langle H_d^0\rangle^2 Q'_{H_d}Q'_N + \langle H_u^0\rangle^2 Q'_{H_u}Q'_N \\ &\quad + \langle S\rangle^2 Q'_N Q'_S) + (\mathbf{m}_\nu^{jj})^2 + M_{N_j}^2 \\ m_{\widetilde{\nu}_{LR}^{ij}}^2 &= (m_{\widetilde{\nu}_{RL}^{ij}}^2)^* \\ &= \mathbf{m}_\nu^{ij}\left[A_{\nu_i}^* + \frac{\mu}{\tan\beta}\left(1 - \left(\frac{\langle H_u^0\rangle}{\langle S\rangle}\right)^2\right)\right]. \quad (8) \end{aligned}$$

Here $M_{L_i}^2$ and $M_{N_i}^2$ are the soft mass terms and A_{ν_i} are the trilinear couplings (assumed diagonal). $\mathbf{m}_\nu$ and μ are given in (3) and (2), respectively. Note that due to the specific $U(1)'$ charge assignments in Table I, some of the terms in (8) are zero. The sneutrino mass eigenstates $\widetilde{\nu}_{1,2}^i$ are given by

$$\begin{pmatrix} \widetilde{\nu}_1^i \\ \widetilde{\nu}_2^i \end{pmatrix} = \begin{pmatrix} \cos\Theta_{\widetilde{\nu}_L-\widetilde{\nu}_R}^i & \sin\Theta_{\widetilde{\nu}_L-\widetilde{\nu}_R}^i \\ -\sin\Theta_{\widetilde{\nu}_L-\widetilde{\nu}_R}^i & \cos\Theta_{\widetilde{\nu}_L-\widetilde{\nu}_R}^i \end{pmatrix} \begin{pmatrix} \widetilde{\nu}_L^i \\ \widetilde{\nu}_R^i \end{pmatrix} \quad (9)$$

with the left-right sneutrino mixing angles $\Theta_{\widetilde{\nu}_L-\widetilde{\nu}_R}^i$:

$$\Theta_{\widetilde{\nu}_L-\widetilde{\nu}_R}^i = \frac{1}{2}\arctan\left(\frac{m_{\widetilde{\nu}_{RL}^{ii}}^2 + m_{\widetilde{\nu}_{LR}^{ii}}^2}{m_{\widetilde{\nu}_{LL}^i}^2 - m_{\widetilde{\nu}_{RR}^i}^2}\right), \quad (10)$$

such that $m_{\widetilde{\nu}_1^i} < m_{\widetilde{\nu}_2^i}$, $i = 1, 2, 3$. In the rest of the paper we will refer to the right-handed sneutrinos as $\widetilde{\nu}_R^i$, $i = 1, 2, 3$ for simplicity, but in the numerical analysis all the mixings are implemented. Note that even though such a mixing is small numerically, it must be retained. The alternative is to introduce mass insertions to obtain most of the decay channels discussed below and `CalcHEP` cannot handle such insertions.

For the numerical analysis, we use the following input values:

$$\mu = 1560\,\text{GeV}, \quad \tan\beta = 0.15, \quad M_R = 10^{16}\,\text{GeV}$$
$$h_\mu = 0.4, \quad M_{L_i} = 2000\,\text{GeV}, \quad A_{\nu_i} = 200\,\text{GeV}$$
$$M_{N_1} = 100\,\text{GeV}, \quad M_{N_2} = 1.2\,\text{TeV}, \quad M_{N_3} = 5\,\text{TeV}$$
$$M_1 = 1400\,\text{GeV}, \quad M_2 = 1600\,\text{GeV}, \quad M_3 = 2\,\text{TeV} \quad (11)$$

where M_1, M_2 and M_3 are the soft gaugino mass terms for $U(1)$, $SU(2)_L$ and $SU(3)$, respectively. For the chosen point in the parameter space, the masses entering the calculations are given in Table II. Clearly, the LSP is $\widetilde{\nu}_e^1$ and the NLSP is $\widetilde{\nu}_\mu^1$, denoted as $\widetilde{\nu}_R^1$ and $\widetilde{\nu}_R^2$ in the rest of the text. The third right-handed sneutrino $\widetilde{\nu}_R^3$ becomes $\widetilde{\nu}_R^2$. The NNLSP is $\widetilde{\chi}_1^0$ as previously chosen. The total widths of these particles are also given in Table III.

We first address the hadronic BBN constraints on several particles in the table, as it is known that late decaying particles may spoil the predictions of BBN and thus need special attention. From Table III, there are only two particles, namely $\widetilde{\chi}_1^0$ and $\widetilde{\nu}_\tau^2$, with lifetimes ~ 1.2 sec and $\sim 10^{-5}$ sec, respectively, which survive and decay after the freeze-out of the NNLSP. In our scenario, the relevant quantity [36] that needs to be evaluated and compared with the observational constraints on light elements like

$m_{\widetilde{\nu}_e^1}$	$m_{\widetilde{\nu}_e^2}$	$m_{\widetilde{\nu}_\mu^1}$	$m_{\widetilde{\nu}_\mu^2}$	$m_{\widetilde{\nu}_\tau^1}$	$m_{\widetilde{\nu}_\tau^2}$
100	2000	1200	2000	2000	5000
$m_{\widetilde{\chi}_1^0}$	$m_{\widetilde{\chi}_2^0}$	$m_{\widetilde{\chi}_3^0}$	$m_{\widetilde{\chi}_4^0}$	$m_{\widetilde{\chi}_5^0}$	$m_{\widetilde{\chi}_6^0}$
1392	1519	1561	1650	2537	2538
$m_{\widetilde{\chi}_1^+}$	$m_{\widetilde{\chi}_2^+}$	$m_{H_1^0}$	$m_{H_2^0}$	$m_{H_3^0}$	$m_{Z'}$
1513	1648	87	2556	5410	2536
$m_{\widetilde{e}_L}$	$m_{\widetilde{e}_R}$	$m_{\widetilde{\mu}_L}$	$m_{\widetilde{\mu}_R}$	$m_{\widetilde{\tau}_L}$	$m_{\widetilde{\tau}_R}$
1999	1999	1999	1999	1999	1999

TABLE II: *The relevant masses in GeV for the chosen parameter set.* $m_{\widetilde{\chi}_a^0}$ $(m_{\widetilde{\chi}_b^+})$ *denotes the mass of the a^{th}(b^{th}) neutralino (chargino) state.* $H_{1,2,3}^0$ *are the physical CP-even neutral Higgs bosons.* $m_{\widetilde{\nu}_e^1}$ *and* $m_{\widetilde{\nu}_\mu^1}$ *denote the masses of the LSP and NLSP refereed as* $m_{\widetilde{\nu}_R^1}$ *and* $m_{\widetilde{\nu}_R^2}$ *in the text.*

$\Gamma_{\widetilde{\nu}_e^1}$	$\Gamma_{\widetilde{\nu}_e^2}$	$\Gamma_{\widetilde{\nu}_\mu^1}$	$\Gamma_{\widetilde{\nu}_\mu^2}$	$\Gamma_{\widetilde{\nu}_\tau^1}$	$\Gamma_{\widetilde{\nu}_\tau^2}$
0	3.95	3.5×10^{-52}	3.95	3.95	6.5×10^{-20}
$\Gamma_{\widetilde{\chi}_1^0}$	$\Gamma_{\widetilde{\chi}_2^0}$	$\Gamma_{\widetilde{\chi}_3^0}$	$\Gamma_{\widetilde{\chi}_4^0}$	$\Gamma_{\widetilde{\chi}_5^0}$	$\Gamma_{\widetilde{\chi}_6^0}$
7.7×10^{-25}	0.30	1.0	1.5	6.2	11.6
$\Gamma_{\widetilde{\chi}_1^+}$	$\Gamma_{\widetilde{\chi}_2^+}$	$\Gamma_{H_1^0}$	$\Gamma_{H_2^0}$	$\Gamma_{H_3^0}$	$\Gamma_{Z'}$
0.13	1.9	0.0041	24.6	27176.5	63.7
$\Gamma_{\widetilde{e}_L}$	$\Gamma_{\widetilde{e}_R}$	$\Gamma_{\widetilde{\mu}_L}$	$\Gamma_{\widetilde{\mu}_R}$	$\Gamma_{\widetilde{\tau}_1}$	$\Gamma_{\widetilde{\tau}_2}$
3.9	1.1×10^{-10}	3.9	4.6×10^{-6}	2.2	1.8

TABLE III: *The relevant total decay widths for the particles in Table II in GeV for the chosen parameter set.* $\Gamma_{\widetilde{\nu}_e^1}$ *and* $\Gamma_{\widetilde{\nu}_\mu^1}$ *denote the decay widths of the LSP and NLSP.*

^{4}He, D, ^{6}Li etc is

$$\eta = \left(\epsilon_{\widetilde{\nu}_R^1} \mathcal{B}(\widetilde{\chi}_1^0 \to \widetilde{\nu}_R^1 q\bar{q} X_1) + \epsilon_{\widetilde{\nu}_R^2} \mathcal{B}(\widetilde{\chi}_1^0 \to \widetilde{\nu}_R^2 q\bar{q} X_2) \right) Y_{\widetilde{\chi}_1^0}$$

where $\epsilon_{\widetilde{\nu}_R^{1,2}}$ are the energies carried by the hadrons and $Y_{\widetilde{\chi}_1^0}$ is the yield variable, defined as $Y_{\widetilde{\chi}_1^0} = n_{\widetilde{\chi}_1^0}/s$ with $n_{\widetilde{\chi}_1^0}$ the number density of $\widetilde{\chi}_1^0$ and s the total entropy density. This quantity is calculated with the help of `MicrOMEGAs`. We also generated all the relevant three-body decays eventually leading to hadronic final states. These are $\widetilde{\chi}_1^0 \to \widetilde{\nu}_R^{1,2} \bar{\nu}_i H_1^0(Z)$ and $\widetilde{\chi}_1^0 \to \widetilde{\nu}_R^{1,2} \ell_i^+ W$. Then H_1^0, Z, and W decay hadronically. We found that $\mathcal{B}(H_1^0 \to q\bar{q}) = 0.95$, $\mathcal{B}(Z \to q\bar{q}) = 0.72$, and $\mathcal{B}(W \to q\bar{q}') = 0.67$. When all of the quantities are entered numerically, the variable η is around 10^{-12} GeV. In the range of the lifetimes of particles, the constraint coming from the overproduction of ^{4}He is relevant. The observational constraint requires $\eta(^4\text{He}) < 10^{-9.47}$ [11], which is satisfied for the $\widetilde{\chi}_1^0$ case. We repeated the analysis for the heaviest right-handed sneutrino $(\widetilde{\nu}_\tau^2)$ and found η even smaller than 10^{-12} GeV.

After insuring that the hadronic BBN constraints are satisfied, we proceed with the relic density calculation. As mentioned earlier, there are two particles, $\widetilde{\nu}_R^1$ and $\widetilde{\nu}_R^2$ as the components of the DM. Including the contributions after freeze-out, the total relic density of the right-handed sneutrinos is given

$$\Omega_{\widetilde{\nu}_R} = \Omega_{\widetilde{\nu}_R^1}^{\texttt{ce}} + \Omega_{\widetilde{\nu}_R^2}^{\texttt{ce}} + \Omega_{\widetilde{\nu}_R}^{\texttt{fo}} \quad (12)$$

where "`ce`" ("`fo`") refers the contributions from decays at chemical equilibrium (after freeze-out). The contribution to the relic density from the heaviest right-handed sneutrino is small and neglected here. Thus, $\Omega_{\widetilde{\nu}_R}^{\texttt{fo}}$ has contributions only from the NNLSP $\widetilde{\chi}_1^0$. It is defined as

$$\frac{\Omega_{\widetilde{\nu}_R}^{\texttt{fo}}}{\Omega_{\widetilde{\chi}_1^0}} = \frac{m_{\widetilde{\nu}_R^1}}{m_{\widetilde{\chi}_1^0}} \mathcal{B}(\widetilde{\chi}_1^0 \to \widetilde{\nu}_R^1 \bar{\nu}_i) + \frac{m_{\widetilde{\nu}_R^2}}{m_{\widetilde{\chi}_1^0}} \mathcal{B}(\widetilde{\chi}_1^0 \to \widetilde{\nu}_R^2 \bar{\nu}_j)$$

$\Omega_{\widetilde{\nu}_R^1}^{\mathtt{ce}} h^2$	$\Omega_{\widetilde{\nu}_R^2}^{\mathtt{ce}} h^2$	$\Omega_{\widetilde{\nu}_R^1}^{\mathtt{fo}} h^2$	$\Omega_{\widetilde{\nu}_R^2}^{\mathtt{fo}} h^2$	$= \Omega_{\widetilde{\nu}_R} h^2$
0.000112	0.0444	0.000929	0.0665	$= 0.1119$

TABLE IV: *The individual contributions to the relic density for the parameter set (11).*

where $i, j = 1, 2, 3$ (we also include the conjugated states). Of course, the sum of the branching ratios has to be unity, *i.e.*, $\sum_{i,j=1}^{3} \left(\mathcal{B}(\widetilde{\chi}_1^0 \to \widetilde{\nu}_R^1 \bar{\nu}_i) + \mathcal{B}(\widetilde{\chi}_1^0 \to \widetilde{\nu}_R^2 \bar{\nu}_j) \right) = 1$. Numerically, we found $\sum_{i,j=1}^{3} \mathcal{B}(\widetilde{\chi}_1^0 \to \widetilde{\nu}_R^1 \bar{\nu}_i) = 0.86$ and $\sum_{i,j=1}^{3} \mathcal{B}(\widetilde{\chi}_1^0 \to \widetilde{\nu}_R^2 \bar{\nu}_i) = 0.14$ in the parameter set (11). $\Omega_{\widetilde{\chi}_1^0}$ is the would-be relic density of NNLSP for the case where it is stable. We have calculated $\Omega_{\widetilde{\chi}_1^0}$ by using the MicrOMEGAs [34] through its CalcHEP interface. Numerically, we found $\Omega_{\widetilde{\chi}_1^0} h^2 = 0.09$ with the usual dimensionless parameter $x_F \equiv T_F / m_{\widetilde{\chi}_1^0} = 1/29.8$. Here h and T_F are the Hubble parameter and the freeze-out temperature. For example, the two most significant contributions to $1/\Omega_{\widetilde{\chi}_1^0}$ from the (co-)annihilation channels are $\widetilde{\chi}_1^0 \widetilde{\chi}_1^0 \to t\bar{t}$ (42%) and $\widetilde{\chi}_1^+ \widetilde{\chi}_1^0 \to t\bar{b}$ (23%).

For the calculation of $\Omega_{\widetilde{\nu}_R^1}^{\mathtt{ce}}$ and $\Omega_{\widetilde{\nu}_R^2}^{\mathtt{ce}}$, the following decay channels are included (conjugated states are not listed):

$$
\begin{aligned}
&\widetilde{\chi}_a^0 \to \bar{\nu}_i \widetilde{\nu}_R^{1,2}, \quad a = 1, \ldots 6, \quad i = 1, 2, 3 \\
&\widetilde{\chi}_b^+ \to \ell \widetilde{\nu}_R^{1,2}, \quad b = 1, 2, \quad \ell = e, \mu, \tau \\
&\widetilde{\ell}_L^+ \to W^+ \widetilde{\nu}_R^{1,2}, \quad \widetilde{\ell}_L = \widetilde{e}_L, \widetilde{\mu}_L, \widetilde{\tau}_1, \widetilde{\tau}_2 \\
&\widetilde{\nu}_\mu^2 \to H_1^0 \widetilde{\nu}_R^{1,2}, \quad \widetilde{\nu}_\tau^1 \to H_1^0 \widetilde{\nu}_R^{1,2}, \\
&\widetilde{\nu}_e^2 \to H_1^0 \widetilde{\nu}_R^2, \quad \widetilde{\nu}_\mu^2 \to Z \widetilde{\nu}_R^2.
\end{aligned} \tag{13}
$$

We performed a complete parameter scan, and found these are the only decay modes which are numerically significant. The individual contributions to the relic density are summarized in Table IV. In the table, we split the freeze-out contribution $\Omega_{\widetilde{\nu}_R}^{\mathtt{fo}}$ into two parts, $\Omega_{\widetilde{\nu}_R^1}^{\mathtt{fo}}$ and $\Omega_{\widetilde{\nu}_R^2}^{\mathtt{fo}}$, which show the contributions of the NNLSP decaying to both the LSP and the NLSP, $\widetilde{\chi}_1^0 \to \bar{\nu}_i \widetilde{\nu}_R^1$, and $\widetilde{\chi}_1^0 \to \bar{\nu}_i \widetilde{\nu}_R^2$, respectively. As can be seen from Table IV, the dominant contributions are coming from $\Omega_{\widetilde{\nu}_R^2}^{\mathtt{ce}}$ (39.7%) and $\Omega_{\widetilde{\nu}_R^2}^{\mathtt{fo}}$ (59.4%) and only $\sim 1\%$ comes from decays to the LSP, as expected. From (10), the mixing angle is inversely proportional to $m_{\widetilde{\nu}_{LL}^i}^2 - m_{\widetilde{\nu}_{RR}^i}^2$. Thus, as the mass difference between left and right handed sneutrinos becomes smaller, their mixing becomes larger. From the fact that $m_{\widetilde{\nu}_R^1} = 100 \text{GeV}$ and $m_{\widetilde{\nu}_R^2} = 1200 \text{GeV}$ as well as $m_{\widetilde{\nu}_L^i} = 2000 \text{GeV}$, the NLSP $\widetilde{\nu}_R^2$ mixes largely with left-handed sneutrino fields and becomes most likely to be produced through the decays in (13). The total relic density is 0.1036, which lies in the 2σ of the WMAP value (with those from the Sloan Digital Sky Survey) [37]:

$$
\Omega_{DM} h^2 = 0.111_{-0.015}^{+0.011} \tag{14}
$$

Having shown that the parameter set of (11) can reproduce the required relic density, we next investigate the positron flux and discuss the PAMELA, ATIC and FERMI-LAT data for the same parameter set.

B. Understanding the PAMELA, ATIC and FERMI-LAT data

Unlike the decays of heavy superpartners, the decay of the NLSP into the LSP proceeds much more slowly as seen from Table III (see also [23]). The reason is as follows. As gauge singlets, the sneutrinos do not couple to gauginos but only to Higgsinos, via

$$
\frac{1}{M_R} \left[S \left(\nu_L \widetilde{H}_u^0 - e_L \widetilde{H}_u^+ \right) + H_u^0 \nu_L \widetilde{S} - H_u^+ e_L \widetilde{S} \right] \mathbf{Y}_\nu \widetilde{\nu}_R, \tag{15}
$$

in which the Yukawa interactions of the Higgsinos are

$$
\begin{aligned}
&h_\mu S \left(\widetilde{H}_u^0 \widetilde{H}_d^0 - \widetilde{H}_u^+ \widetilde{H}_d^- \right) + h_\mu \left(H_u^0 \widetilde{S} \widetilde{H}_d^0 - H_u^+ \widetilde{S} \widetilde{H}_d^- \right) \\
&+ h_\mu \left(\widetilde{S} \widetilde{H}_u^0 H_d^0 - \widetilde{S} \widetilde{H}_u^+ H_d^- \right).
\end{aligned} \tag{16}
$$

These interaction terms show that the exchanges of $\widetilde{H}_u^0$ and $\widetilde{S}$ induce

$$
\widetilde{\nu}_R^2 \to \widetilde{\nu}_R^1 \nu_i \bar{\nu}_j, \tag{17}
$$

and the $\widetilde{H}_u^+$ exchange gives rise to the decay

$$
\widetilde{\nu}_R^2 \to \widetilde{\nu}_R^1 \ell_i^\pm \ell_j^\mp. \tag{18}
$$

The rate of this dileptonic decay is given by

$$
\begin{aligned}
\Gamma_{\ell_i^\pm \ell_j^\mp} &= \frac{1}{(2\pi)^3} \left(\overline{\mathbf{Y}}_\nu^\dagger \overline{\mathbf{Y}}_\nu \right)_{11} \left(\overline{\mathbf{Y}}_\nu \overline{\mathbf{Y}}_\nu^\dagger \right)_{22} \left(\frac{C_a}{\sin\beta} \right)^4 \\
&\times \frac{m_{\widetilde{\nu}_R^2}}{32} \left(\frac{m_{\widetilde{\nu}_R^2}}{m_{\widetilde{\chi}_a^+}} \right)^4 \mathcal{G}_\ell \left(\frac{m_{\widetilde{\chi}_a^+}^2}{m_{\widetilde{\nu}_R^2}^2}, \frac{m_{\widetilde{\nu}_R^1}^2}{m_{\widetilde{\nu}_R^2}^2} \right),
\end{aligned} \tag{19}
$$

after summing over all three lepton generations. Integrating over the Dalitz density gives

$$
\begin{aligned}
\mathcal{G}_\ell(x, y) &= x (y-1) \left[x(5-6x) + y(5x-2) \right] \\
&- 2y^2 \log y - \Big[2(y-x)(x-1) \\
&\times (y+x+xy-3x^2) \log \left(\frac{x-y}{x-1} \right) \Big],
\end{aligned} \tag{20}
$$

which appears in (19) with the indicated arguments. The two chargino states $\widetilde{\chi}_a^+$ ($a = 1, 2$) with masses $m_{\widetilde{\chi}_a^+}$, also appear in the decay rate via $\widetilde{H}_u^+ = C_1 P_R \widetilde{\chi}_1^+ + C_2 P_R \widetilde{\chi}_2^+$, in which

$$
\frac{C_1 C_2}{C_2^2 - C_1^2} = \frac{r_{W2}(\sin\beta + r_{\mu 2} \cos\beta)}{1 - r_{\mu 2}^2 + r_{W2}^2 \cos 2\beta} \tag{21}
$$

where $C_2 = \sqrt{1 - C_1^2}$, $r_{W2} = \sqrt{2}M_W/M_2$, $r_{\mu 2} = h_\mu \langle S \rangle / M_2$, and M_2 is the $SU(2)_L$ gaugino mass.

Various analyses [9] of PAMELA and other satellite data suggest that, rather model independently, the DM candidate must have a lifetime of $\sim 10^{26}$ sec. This is consistent with the dileptonic decay rate (19) in that for the parameter choice in (11), one finds

$$\Gamma_{\ell_i^\pm \ell_j^\mp} = 6.8 \times 10^{-51} \text{ GeV}, \qquad (22)$$

leading to a $\sim 10^{26}$ sec lifetime. This arises from the small $\langle S \rangle / M_{GUT}$ ratio that sets the neutrino mass scale. One notices that the value of the rate involves the sum of all three generations of charged leptons ($i, j = 1, 2, 3$) as well as all the conjugated modes. Note that there is no contribution to the positron production from the third right-handed sneutrino since it only lives 10^{-5} sec and thus decays much faster.

In contrast to the case of the MSSM with right-handed neutrinos [11, 23], the μ term and the neutrino Yukawa couplings are induced dynamically in our model. The two models also differ in terms of the predicted correlation between the neutrino masses (3) and the dileptonic decay rate (19). In the MSSM, these quantities are directly correlated via the Yukawa couplings $\overline{\mathbf{Y}}_\nu \sim \mathcal{O}(10^{-13})$. In our model, the rate involves both $\langle S \rangle / M_{GUT}$ and $m_{\widetilde{\nu}_R^2} / m_{\widetilde{H}_u}$, and, in the heavy Higgsino regime where $m_{\widetilde{\chi}_2^+} \simeq m_{\widetilde{H}_u} \simeq \mu \gg M_2, M_W$, it scales as $(m_{\widetilde{\nu}_R^2} / m_{\widetilde{\nu}_R^1})^4$, not as $(\langle S \rangle / M_{GUT})^4$. Hence, in the large μ limit there is only a mild dependence on $m_{\widetilde{H}_u}$, and the "see-saw scale" that suppresses the neutrino masses is then independent of the scale that governs the NLSP decays. However, in this regime the DM lifetime is longer than 10^{26} sec, and hence the heavy Higgsino regime is not particularly preferred given present data.

We now crystallize the qualitative approach presented above with a more detailed calculation of the positron flux originating from the decay (18) with the decay width (19). We follow the procedure in [9], to which we refer the reader for further details. The source term of the diffusion equation is

$$Q_{\ell_i^\pm}(E_{\ell_i^\pm}, \mathbf{r}) = \frac{n_{\text{NLSP}}}{\tau_{\text{NLSP}}} \frac{dN_{\ell_i^\pm}}{dE_{\ell_i^\pm}}, \qquad (23)$$

where n_{NLSP} is the number density of the NLSP, τ_{NLSP} is the lifetime (which will be set as a free parameter to be fit), and $dN_{\ell_i^\pm}/dE_{\ell_i^\pm}$ is the energy distribution of $\ell_i^\pm$ from the decay $\widetilde{\nu}_R^2 \to \widetilde{\nu}_R^1 \ell_i^\pm \ell_j^\mp$. Before proceeding to evaluate $dN_{\ell_i^\pm}/dE_{\ell_i^\pm}$, we first determine τ_{NLSP}.

Since both the LSP and the NLSP are components of the DM, other particles decay to either of them. Then, the ratio of the number densities of the LSP and NLSP should be equal to the ratios of the branching rates into either state. Explicitly,

$$\frac{n_{\text{LSP}}}{n_{\text{NLSP}}} = \frac{\sum_{A,B} \mathcal{B}(A \to B\,\widetilde{\nu}_R^1)}{\sum_{A',B'} \mathcal{B}(A' \to B'\,\widetilde{\nu}_R^2)} \equiv \alpha \qquad (24)$$

where A, B, A', and B' represent all possible particles of the model and the right hand side is known once we fix the free parameters. For example, numerical evaluation yields, $\sum_{A,B} \mathcal{B}(A \to B\,\widetilde{\nu}_R^1) = 0.0718$ and $\sum_{A,B} \mathcal{B}(A \to B\,\widetilde{\nu}_R^2) = 0.428$ for the particular parameter set considered here. There are two unknown in the left hand side of (24). The second relation needed arises from the mass density of the DM, $\rho_{\text{DM}}(r)$, as

$$m_{\widetilde{\nu}_R^1} n_{\text{LSP}} + m_{\widetilde{\nu}_R^2} n_{\text{NLSP}} = \rho_{\text{DM}}(r) \qquad (25)$$

where $\rho_{\text{DM}}(\mathbf{r})$ is further parametrized by adopting the Navarro-Frank-White density profile [38]. For the diffusion parameters, we use the three sets from models M1, M2 and MED [9].

We return to the evaluation of the $dN_{\ell_i^\pm}/dE_{\ell_i^\pm}$ term. The definition and normalization of this term depends on whether the positron/electron pair is produced directly from the decay $\widetilde{\nu}_R^2 \to \widetilde{\nu}_R^1 e^- e^+$ (that is, $i = j = 1$) or through some cascade decays. Our numerical analysis shows that in addition to the direct $e^- e^+$ production case, the $e^\pm \mu^\mp$ has also significant decay width. In this case the muon $\mu^\pm$ will decay further as $\mu^\pm \to \nu_\mu e^\pm \nu_e$ where the appropriate combinations of ν_μ and ν_e should be understood based on the charge of μ or e. In principle, the τ lepton can also be produced directly which then requires two cascade decays to get the positron/electron pair. So, we consider direct productions of positron/electron, or indirect production only through the muon cascade. The details of how to treat the cascade productions of positron/electron from the muon cascade can be found for example in [39]. If the electron/positron pair is produced directly, then the $dN_{\ell_i^\pm}/dE_{\ell_i^\pm}$ is given

$$\frac{dN_{e^\pm}^{[e^- e^+]}}{dE_{e^\pm}} = \frac{1}{\Gamma_{e^+ e^-}} \int dE_{e^\mp} \frac{d^2\Gamma}{dE_{e^+} dE_{e^-}}. \qquad (26)$$

where $\Gamma_{e^+ e^-}$ is the decay width for the direct electron/positron production case. If positron/electron is produced from the decay $\widetilde{\nu}_R^2 \to \widetilde{\nu}_R^1 e^\pm \mu^\mp$ followed by the decay of the muon $\mu^\mp \to \nu_\mu e^\mp \nu_e$, we write the dN/dE term for the positron only for notational simplicity (the electron case is very similar):

$$\frac{dN_{e^+}^{[e^\pm \mu^\mp]}}{dE_{e^+}} = \frac{1}{N_{e^\pm \mu^\mp}} \left(\frac{d\Gamma^{e^+ \mu^-}}{dE_{e^+}} + \int dE_{\mu^+} \frac{d^2\Gamma^{e^- \mu^+}}{dE_{e^+} dE_{\mu^+}} \right) \quad (27)$$

where the second term is represented generically after carrying out the integral over the electron energy E_{e^-}. In this term, the muon decays further to a positron with energy E_{e^+}. The combined contribution is included in the second term. The first term corresponds to the case where the leptons in the final state are $e^+ \mu^-$ so that there is no further decay considered for the positron case. The normalization factor $N_{e^\pm \mu^\mp}$ is given by

$$N_{e^\pm \mu^\mp} = \Gamma_{e^+ \mu^-} + \int dE_{e^+} dE_{\mu^+} \frac{d^2\Gamma^{e^- \mu^+}}{dE_{e^+} dE_{\mu^+}} \qquad (28)$$

The solution of the diffusion equation for the flux $\Phi_{e^\pm}$ is given in terms of the Green's function in [9] as

$$\Phi_{e^\pm}(E_{e^\pm}) = \frac{c}{4\pi\, m_{\text{eff}}\tau_{\text{NLSP}}} \int dE\, G(E, E_{e^\pm}) \frac{dN_{e^\pm}}{dE} \quad (29)$$

where either (26) or (27) should be used for the $dN_{e^\pm}/dE$ term depending on the relevant decay mode. Here $m_{\text{eff}} = \alpha\, m_{\widetilde{\nu}_R^1} + m_{\widetilde{\nu}_R^2}$ is an effective mass term originating from the solution of (24) and (25). We further approximate the Green's function as in [40] to maximize computational efficiency.

The flux $\Phi_{e^\pm}$ obtained as a solution of the diffusion equation is then used to define the ratio for the positron flux $R_{e^\pm}$:

$$R_{e^\pm} = \frac{\Phi_{e^+}^{\text{tot}}}{\Phi_{e^-}^{\text{tot}} + \Phi_{e^+}^{\text{tot}}}, \quad (30)$$

where $\Phi_{e^\pm}^{\text{tot}}$ is the sum of $\Phi_{e^\pm}$ and the background flux in our galaxy and we define $\Phi_{e^\pm}^{\text{tot}}$

$$\Phi_{e^-}^{\text{tot}} = \Phi_{e^-} + \kappa^- \left(\Phi_{e^-}^{\text{prim}} + \Phi_{e^-}^{\text{sec}}\right),$$
$$\Phi_{e^+}^{\text{tot}} = \Phi_{e^+} + \kappa^+ \Phi_{e^+}^{\text{sec}}, \quad (31)$$

where $\kappa^\pm$ represents the uncertainties in the $e^+(e^-)$ background. $(\kappa^-, \kappa^+) = (0.7, 0.9)$ is used in the numerical study. The following electron and positron backgrounds $(\Phi_{e^-}^{\text{prim}}, \Phi_{e^\mp}^{\text{sec}})$ in our galaxy are approximated as [41] in units of $(\text{GeV cm}^2 \sec \text{sr})^{-1}$

$$\Phi_{e^-}^{\text{prim}} = \frac{0.16E^{-1.1}}{1 + 11E^{0.9} + 3.2E^{2.15}}$$
$$\Phi_{e^-}^{\text{sec}} = \frac{0.7E^{0.7}}{1 + 110E^{1.5} + 600E^{2.9} + 580E^{4.2}}$$
$$\Phi_{e^+}^{\text{sec}} = \frac{4.5E^{0.7}}{1 + 650E^{2.3} + 1500E^{4.2}} \quad (32)$$

The quantity $R_{e^\pm}$ in (30) can be used to compare with the PAMELA data. Similarly the total flux $\Phi_{e^-}^{\text{tot}} + \Phi_{e^+}^{\text{tot}}$ scaled by $E_{e^\pm}^3$ is the relevant observable for the ATIC and the FERMI-LAT experiments.

Our results for the positron flux are shown in Figs. (1), (2), and (3) as the ratio R_{e^+} as a function of the positron energy E_{e^+} for each propagation model M1, M2, and MED, respectively. The direct and indirect production of the positron as well as the expected background are shown separately. The figures show that the models M1 and MED fit much better than the M2 model. The fitted curves significantly deviate from the PAMELA data (shown in the figures) for energies less than about 5 GeV but are consistent with the experimental data for $E > 5$ GeV. The fitted values of the lifetimes are $\mathcal{O}(10^{26})$ sec, which are in the expected range. The lifetimes for the M1 and MED models are close to each other, and the value is only slightly smaller for the M2 model. Note also that the constraint on the lifetime of the decaying DM from the cosmic microwave background (CMB)
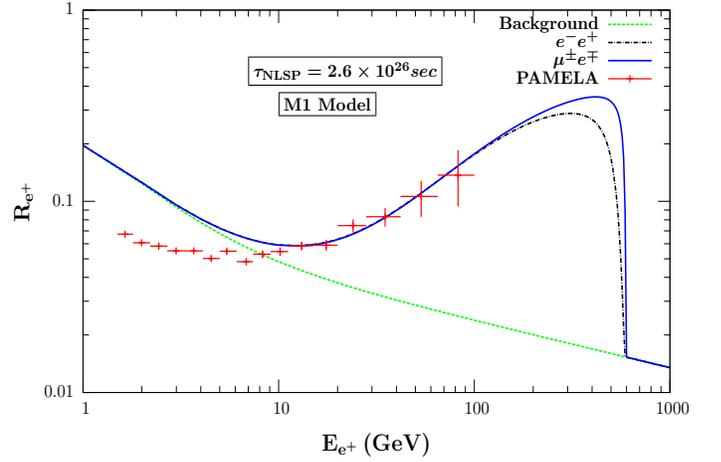

FIG. 1: The positron flux R_{e^+} as a function of positron energy in the M1 propagation model. The direct positron channel (e^-e^+) and the indirect one through muon decay $(\mu^\pm e^\mp)$ are shown separately. The background and the PAMELA data are also shown. The fitted lifetime of NLSP is also indicated.
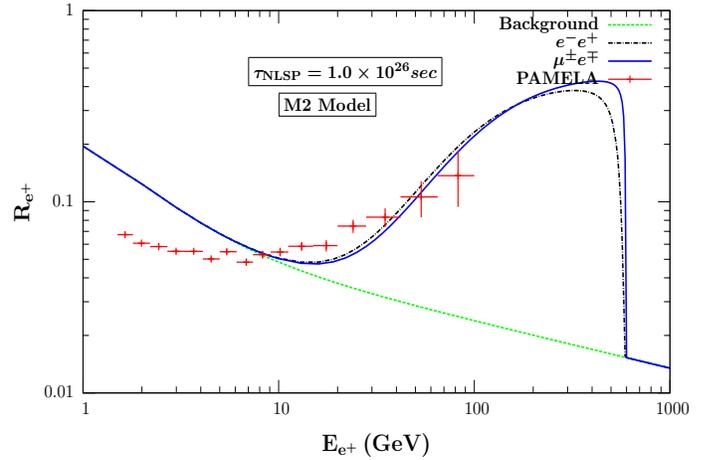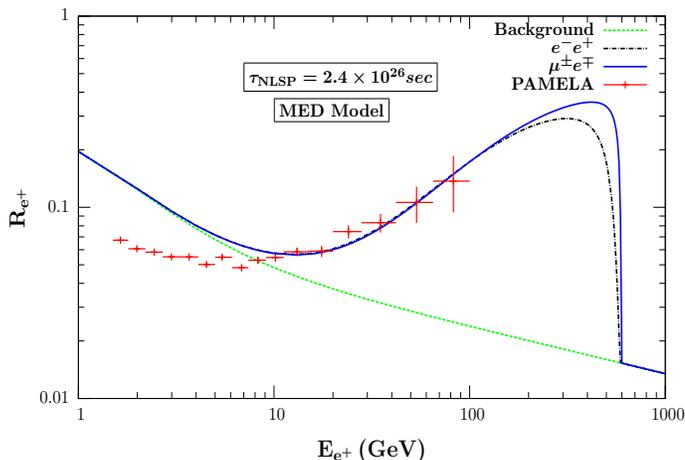

FIG. 2: The positron flux R_{e^+} as a function of positron energy in the M2 propagation model. The direct positron channel (e^-e^+) and the indirect one through muon decay $(\mu^\pm e^\mp)$ are shown separately. The background and the PAMELA data are also shown. The fitted lifetime of NLSP is also indicated.

is analysed in [42], and our results obey the lower bounds. The positron emitted through the $\mu^\pm e^\mp$ channel deviates only from the direct channel part of the high energy tail.

Similar graphs are shown in Figs. (4), (5), and (6) for the total flux scaled by the positron energy $E_{e^\pm}^3$ for the propagation models M1, M2, and MED, respectively. Again the direct and indirect production of the positron as well as the expected background are shown separately. The ATIC and the FERMI-LAT data are also included. As seen from the figures, our signal is a reasonably good fit to the ATIC and FERMI data. Our signal explains the FERMI-LAT data very well up to ~ 400 GeV for the $e^\pm e^\mp$ case and gets even better for the $\mu^\pm e^\mp$ case, where the signal is consistent up to ~ 500 GeV. In the ATIC case, the signal explains the low energy as well as the

FIG. 3: The positron flux R_{e^+} as a function of positron energy in the MED propagation model. The direct positron channel (e^-e^+) and the indirect one through muon decay $(\mu^\pm e^\mp)$ are shown separately. The background and the PAMELA data are also shown. The fitted lifetime of NLSP is also indicated.
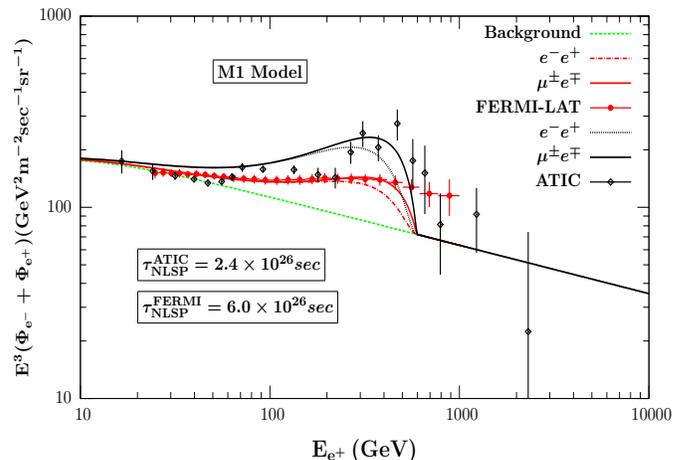

FIG. 4: The total flux scaled by $E_{e^\pm}^3$ as a function of the positron energy in the M1 propagation model. Both the direct positron channel (e^-e^+) and the indirect one through muon decay $(\mu^\pm e^\mp)$ are shown separately. The background and the ATIC and FERMI-LAT data are also shown. The fitted lifetimes of NLSP for each data are also indicated.

peak regions better than the intermediate enery interval. Once again, considering the $\mu^\pm e^\mp$ mode makes the situation better in the end-region. In either case (ATIC or FERMI-LAT), the signal would fit better especially in the high energy region for another set of parameter values. For example, a bigger gap between the LSP and NLSP mass would allow more energetic $e^\pm$ which would shift the dying tail of the signal to the right.

Unlike the PAMELA case, where M1 and MED scenarios are favored, the M2 model works better for ATIC, while the FERMI-LAT data slightly favors the M1 and MED models. The fitted lifetimes for the ATIC data are very close for the propagation models and are also quite consistent with the ones for the PAMELA case (especially for the M1 and MED models). On the other hand, the lifetimes for the FERMI-LAT data are the same for the three models considered (the fitted curves are less sensitive to the types of the model used as long as the lifetimes are in the $(5.4 - 6.0) \times 10^{26}$ sec range). For the M1 and MED models, the FERMI-LAT data requires lifetimes about twice bigger than than the ones for the ATIC and PAMELA cases. The ratio is bigger for the M2 propagation model.

From the results, we can conclude that it is possible to satisfactorily explain the PAMELA+ATIC data simultaneously (except the data in the 100-200 GeV range for the ATIC case) with a consistent lifetime for the DM. It is also possible to explain the FERMI-LAT data, which requires a slightly larger lifetime for the DM and works well for energies up to 500 GeV.

Having discussed the electron/positron excess as well as the total flux, we now consider briefly the issue that no significant excess was observed in the anti-proton flux [10]. Unlike the case of the leptonic decays, the hadronic decays are generated only through the F-term interactions in the superpotential. The relevant interaction

terms in the Lagrangian are given by

$$\mathcal{L} \sim \left(\overline{\mathbf{Y}}_\nu^\dagger \overline{\mathbf{Y}}_\nu\right)_{21} \left(\frac{v}{\sin\beta}\right) \left(\mathcal{R}^{-1}\right)_{ui} H_i^0 \widetilde{\nu}_R^{2\star} \widetilde{\nu}_R^1 + \text{H. c.}, \quad (33)$$

in which H_i^0 $(i = 1, \ldots, 3)$ are the neutral CP-even Higgs bosons and $\mathcal{R}_{ui}$ is the fraction of H_i^0 in H_u^0 [43]. Higgs bosons H_i^0 produced in the $\widetilde{\nu}_R^2$ decay [23] further decay into pairs of quarks (including top quark pairs as suggested by the mass spectrum in (11) and in Table II, gauge bosons, and Higgs bosons. The decay rate to
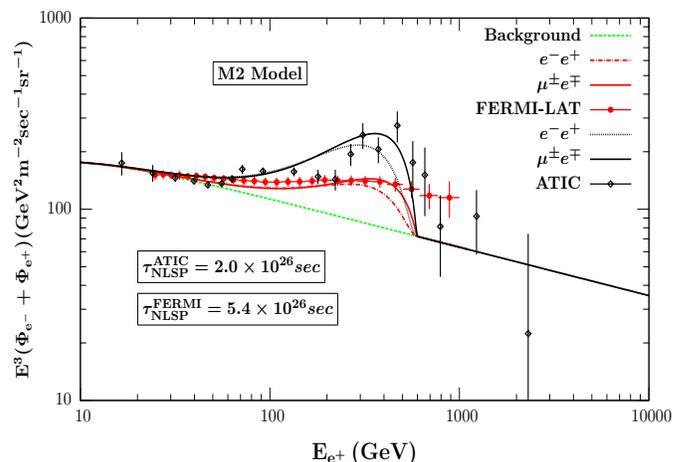

FIG. 5: The total flux scaled by $E_{e^\pm}^3$ as a function of the positron energy in the M2 propagation model. Both the direct positron channel (e^-e^+) and the indirect one through muon decay $(\mu^\pm e^\mp)$ are shown separately. The background and the ATIC and FERMI-LAT data are also shown. The fitted lifetimes of NLSP for each data are also indicated.
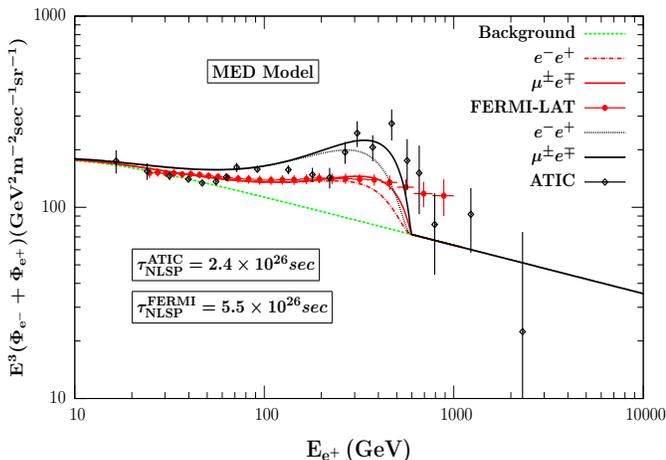
FIG. 6: The total flux scaled by $E_{e\pm}^3$ as a function of the positron energy in the M2 propagation model. Both the direct positron channel (e^-e^+) and the indirect one through muon decay ($\mu^\pm e^\mp$) are shown separately. The background and the ATIC and FERMI-LAT data are also shown. The fitted lifetimes of NLSP for each data are also indicated.

quarks is

$$
\begin{aligned}
\Gamma_{q\bar{q}} &= \frac{N_C}{(2\pi)^3} \left(\overline{\mathbf{Y}}_\nu^\dagger \overline{\mathbf{Y}}_\nu\right)_{12} \left(\overline{\mathbf{Y}}_\nu^\dagger \overline{\mathbf{Y}}_\nu\right)_{21} \sum_{i=1}^3 \left(\frac{\mathcal{R}_{ui}}{\sin\beta}\right)^4 \\
&\times \frac{m_{\widetilde{\nu}_R^2}}{32} \left(\frac{m_q}{m_{\widetilde{\nu}_R^2}}\right)^2 \mathcal{G}_q \left(\frac{M_{H_i^0}^2}{m_{\widetilde{\nu}_R^2}^2}, \frac{m_{\widetilde{\nu}_R^1}^2}{m_{\widetilde{\nu}_R^2}^2}\right).
\end{aligned} \tag{34}
$$

The integrated Dalitz density has the functional form

$$
\begin{aligned}
\mathcal{G}_q(x,y) &= -4(1-y) + \alpha \log y + \left[\frac{1}{\beta}\left(2\beta^2 - \gamma\right)\right. \\
&\left. \times \log\left(\frac{\gamma + (1-y)\beta}{\gamma - (1-y)\beta}\right)\right]
\end{aligned} \tag{35}
$$

with $\alpha = -2x + (1+y)$, $\beta^2 = -x^2 - x\alpha + \gamma$, and $\gamma = (1-y)^2 - x(1+y)$.

The light quarks are produced directly or indirectly through heavy quark, gauge boson, and Higgs boson decays, and hadronize to produce protons and anti-protons. An inspection of (34) and (19) shows that the anti-proton signal is suppressed compared to the positron signal by a kinematic factor of order $\sim 10 m_q^2/m_{\widetilde{\nu}_R^2}^2$, which is $\mathcal{O}\left(10^{-10}\right)$ for u, d quarks and $\mathcal{O}\left(10^{-4}\right)$ for b quarks, as needed for consistency with PAMELA [10].

However, the Higgs bosons that are produced in NLSP to LSP decays fragment efficiently into gauge bosons and top quarks, which in turn give off light quarks and antiquarks with no apparent Yukawa suppression. Moreover, the leptons produced with the rate given in (19) can give rise to hadronic final states at the loop level. These indirect contributions are expected to yield anti-protons with an efficiency around 10% [23, 44].

The needed suppression of the anti-proton flux with respect to the positron flux can stem from various effects, such as the interaction strengths in (33). One way to suppress $\Gamma_{q\bar{q}}$ with respect to $\Gamma_{l^+l^-}$ is to have [23]

$$
\left|\left(\mathbf{Y}_\nu^\dagger \mathbf{Y}_\nu\right)_{21}\right|^2 \lesssim 10^{-4} \left(\mathbf{Y}_\nu^\dagger \mathbf{Y}_\nu\right)_{11} \left(\mathbf{Y}_\nu \mathbf{Y}_\nu^\dagger\right)_{22} \tag{36}
$$

which imposes an overall suppression on the flavor-changing entries of the neutrino Yukawa matrices with respect to the flavor-conserving entries. A justification or realization of such a structure would in principle require a detailed knowledge of the flavor structure of (3). However, it is worth noting that there is no direct correspondence in general between the right-handed neutrino and the active (left-handed) neutrino sectors, which can lend credence for the needed suppression.

IV. CONCLUSIONS

We have presented a simple extension of the MSSM with an additional $U(1)'$ gauge symmetry that couples predominantly to Higgs fields. While other sneutrino dark matter models have been proposed to explain the cosmic ray observations, the model presented here does so while also resolving the naturalness problems of the MSSM. In this model, an electroweak scale μ term and appropriately suppressed Dirac neutrino masses are generated upon $U(1)'$ breaking. The right-handed sneutrinos $\widetilde{\nu}_R^1$ and $\widetilde{\nu}_R^2$ are the lightest and next-to-lightest superpartners, allowing for a natural explanation of PAMELA and other experiments like ATIC and FERMI-LAT in the context of sneutrino dark matter.

A complete study of the DM relic density in this model includes contributions from the LSP and the NLSP, which is essentially stable with respect to the lifetime of the universe. We also analysed the contributions coming from late decaying particles, *i.e.*, particles that decay after freeze-out. For the parameter set in (11), we obtain 0.1036 for the total relic density of right-handed sneutrino, consistent with the current WMAP value.

We then discussed the PAMELA, ATIC and FERMI-LAT data, considering $\widetilde{\nu}_R^2 \to \widetilde{\nu}_R^1 l_i^\pm l_j^\mp$ as the source decay for the observed positron excess. The possibility of producing a final positron through muon is also discussed separately. The suppression of the anti-proton flux compared to the positron flux suggests the model-building constraint that the flavor-changing entries of the neutrino Yukawa coupling matrix are suppressed with respect to the flavor-conserving entries. The fitted lifetimes for the DM, of the order of 10^{26} sec, fit the PAMELA data well for positron energies greater than 5 GeV, as well as the ATIC and FERMI-LAT cases. The fit is better for the M1 and MED models described in the text. It can be concluded from the values of the fitted lifetimes that it maybe possible to explain the PAMELA+ATIC and FERMI-LAT data simultaneously in the corresponding energy ranges, though the FERMI-LAT data requires a

slightly larger lifetime values for the DM. In principle, it is foreseeable that a better scan of the model parameters as well as implementing an improved fitting procedure could offer an even closer simultaneous explanation of these three sets of experimental data.

V. ACKNOWLEDGEMENTS

[1] E. Komatsu *et al.* [WMAP Collaboration], Astrophys. J. Suppl. **180**, 330 (2009) [arXiv:0803.0547 [astro-ph]].

[2] O. Adriani *et al.* [PAMELA Collaboration], Nature **458**, 607 (2009) [arXiv:0810.4995 [astro-ph]].

[3] S. Torii *et al.* [PPB-BETS Collaboration], arXiv:0809.0760 [astro-ph].

[4] F. Aharonian *et al.* [H.E.S.S. Collaboration], Phys. Rev. Lett. **101**, 261104 (2008) [arXiv:0811.3894 [astro-ph]].

[5] A. A. Abdo *et al.* [The Fermi LAT Collaboration], Phys. Rev. Lett. **102**, 181101 (2009) [arXiv:0905.0025 [astro-ph.HE]].

[6] S. Chang and L. Goodenough, arXiv:0908.2429 [astro-ph.HE]; P. Scott, J. Conrad, J. Edsjo, L. Bergstrom, C. Farnier and Y. Akrami, arXiv:0909.3300 [astro-ph.CO]; K. Y. Choi and C. E. Yaguna, arXiv:0906.0736 [hep-ph].

[7] T. Kobayashi, Y. Komori, K. Yoshida and J. Nishimura, Astrophys. J. **601**, 340 (2004) [arXiv:astro-ph/0308470]; D. Hooper, P. Blasi and P. D. Serpico, JCAP **0901**, 025 (2009) [arXiv:0810.1527 [astro-ph]]; H. Yuksel, M. D. Kistler and T. Stanev, arXiv:0810.2784 [astro-ph]; S. Profumo, arXiv:0812.4457 [astro-ph]; K. Ioka, arXiv:0812.4851 [astro-ph]; N. J. Shaviv, E. Nakar and T. Piran, arXiv:0902.0376 [astro-ph.HE]; D. Malyshev, I. Cholis and J. Gelfand, arXiv:0903.1310 [astro-ph.HE]; N. Kawanaka, K. Ioka and M. M. Nojiri, arXiv:0903.3782 [astro-ph.HE]; Y. Fujita, K. Kohri, R. Yamazaki and K. Ioka, arXiv:0903.5298 [astro-ph.HE].

[8] V. Barger, W. Y. Keung, D. Marfatia and G. Shaughnessy, Phys. Lett. B **672**, 141 (2009) [arXiv:0809.0162 [hep-ph]]; M. Cirelli, M. Kadastik, M. Raidal and A. Strumia, Nucl. Phys. B **813**, 1 (2009) [arXiv:0809.2409 [hep-ph]]; L. Bergstrom, T. Bringmann and J. Edsjo, Phys. Rev. D **78**, 103520 (2008) [arXiv:0808.3725 [astro-ph]]; G. Olivares, F. Atrio-Barandela and D. Pavon, Phys. Rev. D **77**, 103520 (2008) [arXiv:0801.4517 [astro-ph]]; M. Cirelli and A. Strumia, arXiv:0808.3867 [astro-ph]; J. H. Huh, J. E. Kim and B. Kyae, arXiv:0809.2601 [hep-ph]; I. Cholis, D. P. Finkbeiner, L. Goodenough and N. Weiner, arXiv:0810.5344 [astro-ph]; N. Arkani-Hamed, D. P. Finkbeiner, T. R. Slatyer and N. Weiner, Phys. Rev. D **79**, 015014 (2009) [arXiv:0810.0713 [hep-ph]]; J. Hisano, M. Kawasaki, K. Kohri and K. Nakayama, Phys. Rev. D **79**, 063514 (2009) [arXiv:0810.1892 [hep-ph]]; M. Fairbairn and J. Zupan, arXiv:0810.4147 [hep-ph]; A. E. Nelson and C. Spitzer, arXiv:0810.5167 [hep-ph]; D. Feldman, Z. Liu and P. Nath, Phys. Rev. D **79**, 063509 (2009) [arXiv:0810.5762 [hep-ph]]; Y. Bai and Z. Han, arXiv:0811.0387 [hep-ph]; J. Zhang, X. J. Bi, J. Liu, S. M. Liu, P. f. Yin, Q. Yuan and S. H. Zhu, arXiv:0812.0522 [astro-ph]. W. Shepherd, T. M. P. Tait and G. Zaharijas, arXiv:0901.2125 [hep-ph]; S. C. Park and J. Shu, arXiv:0901.0720 [hep-ph]; I. Z. Rothstein, T. Schwetz and J. Zupan, arXiv:0903.3116 [astro-ph.HE]; D. S. M. Alves, S. R. Behbahani, P. Schuster and J. G. Wacker, arXiv:0903.3945 [hep-ph]; V. Barger, Y. Gao, W. Y. Keung, D. Marfatia and G. Shaughnessy, arXiv:0904.2001 [hep-ph]; J. D. March-Russell and S. M. West, Phys. Lett. B **676**, 133 (2009); J. March-Russell, S. M. West, D. Cumberbatch and D. Hooper, JHEP **0807**, 058 (2008).

[9] C. R. Chen, F. Takahashi and T. T. Yanagida, Phys. Lett. B **671**, 71 (2009) [arXiv:0809.0792 [hep-ph]]; P. f. Yin, Q. Yuan, J. Liu, J. Zhang, X. j. Bi and S. h. Zhu, Phys. Rev. D **79**, 023512 (2009) [arXiv:0811.0176 [hep-ph]]; K. Hamaguchi, E. Nakamura, S. Shirai and T. T. Yanagida, arXiv:0811.0737 [hep-ph]; A. Ibarra and D. Tran, JCAP **0902**, 021 (2009) [arXiv:0811.1555 [hep-ph]]; C. R. Chen, M. M. Nojiri, F. Takahashi and T. T. Yanagida, arXiv:0811.3357 [astro-ph]; S. De Lope Amigo, W. Y. Cheung, Z. Huang and S. P. Ng, arXiv:0812.4016 [hep-ph]; C. R. Chen, K. Hamaguchi, M. M. Nojiri, F. Takahashi and S. Torii, arXiv:0812.4200 [astro-ph]; F. Takahashi and E. Komatsu, arXiv:0901.1915 [astro-ph]; C. H. Chen, C. Q. Geng and D. V. Zhuridov, arXiv:0901.2681 [hep-ph]; K. Cheung, P. Y. Tseng and T. C. Yuan, arXiv:0902.4035 [hep-ph]; K. Ishiwata, S. Matsumoto and T. Moroi, arXiv:0903.0242 [hep-ph].

[10] O. Adriani *et al.*, Phys. Rev. Lett. **102**, 051101 (2009) [arXiv:0810.4994 [astro-ph]].

[11] T. Asaka, K. Ishiwata and T. Moroi, Phys. Rev. D **73**, 051301 (2006) [arXiv:hep-ph/0512118]; Phys. Rev. D **75**, 065001 (2007) [arXiv:hep-ph/0612211].

[12] F. Deppisch and A. Pilaftsis, JHEP **0810**, 080 (2008) [arXiv:0808.0490 [hep-ph]].

[13] J. McDonald, JCAP **0701**, 001 (2007) [arXiv:hep-ph/0609126].

[14] H. S. Lee, K. T. Matchev and S. Nasri, Phys. Rev. D **76**, 041302 (2007) [arXiv:hep-ph/0702223].

[15] D. G. Cerdeno, C. Munoz and O. Seto, Phys. Rev. D **79**, 023510 (2009) [arXiv:0807.3029 [hep-ph]].

[16] D. G. Cerdeno and O. Seto, arXiv:0903.4677 [hep-ph].

[17] C. R. Chen and F. Takahashi, JCAP **0902**, 004 (2009) [arXiv:0810.4110 [hep-ph]].

[18] R. Allahverdi, B. Dutta, K. Richardson-McDaniel and Y. Santoso, Phys. Rev. D **79**, 075005 (2009) [arXiv:0812.2196 [hep-ph]]; arXiv:0902.3463 [hep-ph]; B. Dutta, L. Leblond and K. Sinha, arXiv:0904.3773 [hep-ph].

[19] E. Ma, arXiv:0904.4450 [hep-ph].

[20] I. Gogoladze, N. Okada and Q. Shafi, arXiv:0904.2201 [hep-ph].

[21] X. J. Bi, X. G. He and Q. Yuan, arXiv:0903.0122 [hep-ph]; B. Kyae, arXiv:0902.0071 [hep-ph].

[22] H. S. Goh, L. J. Hall and P. Kumar, arXiv:0902.0814 [hep-ph].

[23] M. Pospelov and M. Trott, JHEP **0904**, 044 (2009) [arXiv:0812.0432 [hep-ph]].

[24] J. E. Kim and H. P. Nilles, Phys. Lett. B **138**, 150 (1984).

[25] S. M. Barr, Phys. Rev. Lett. **55** (1985) 2778; F. del Aguila, G. A. Blair, M. Daniel and G. G. Ross, Nucl. Phys. B **272** (1986) 413; J. L. Hewett and T. G. Rizzo, Phys. Rept. **183**, 193 (1989); M. Cvetic and P. Langacker, Phys. Rev. D **54**, 3570 (1996) [arXiv:hep-ph/9511378]; G. Cleaver, M. Cvetic, J. R. Espinosa, L. L. Everett and P. Langacker, Phys. Rev. D **57**, 2701 (1998) [arXiv:hep-ph/9705391]; Nucl. Phys. B **525**, 3 (1998) [arXiv:hep-th/9711178]; D. M. Ghilencea, L. E. Ibanez, N. Irges and F. Quevedo, JHEP **0208** (2002) 016 [arXiv:hep-ph/0205083]; S. F. King, S. Moretti and R. Nevzorov, Phys. Rev. D **73** (2006) 035009 [arXiv:hep-ph/0510419].

[26] M. Cvetic, D. A. Demir, J. R. Espinosa, L. L. Everett and P. Langacker, Phys. Rev. D **56**, 2861 (1997) [Erratum-ibid. D **58**, 119905 (1998)] [arXiv:hep-ph/9703317].

[27] D. A. Demir and Y. Farzan, JHEP **0603**, 010 (2006) [arXiv:hep-ph/0601096].

[28] D. A. Demir, L. L. Everett and P. Langacker, Phys. Rev. Lett. **100**, 091804 (2008) [arXiv:0712.1341 [hep-ph]].

[29] D. A. Demir, G. L. Kane and T. T. Wang, Phys. Rev. D **72**, 015012 (2005) [arXiv:hep-ph/0503290].

[30] A. Ali, D. A. Demir, M. Frank and I. Turan, arXiv:0902.3826 [hep-ph].

[31] D. Hooper, J. March-Russell and S. M. West, Phys. Lett. B **605** (2005) 228; C. Arina and N. Fornengo, JHEP **0711** (2007) 029.

[32] See the URL: http://theory.sinp.msu.ru/~pukhov/calchep.html; A. Pukhov, arXiv:hep-ph/0412191.

[33] A. Semenov, arXiv:0805.0555 [hep-ph]; A. Semenov, Comput. Phys. Commun. **115**, 124 (1998).

[34] G. Belanger, F. Boudjema, A. Pukhov and A. Semenov, Comput. Phys. Commun. **180**, 747 (2009) [arXiv:0803.2360 [hep-ph]]; G. Belanger, F. Boudjema, A. Pukhov and A. Semenov, Comput. Phys. Commun. **176**, 367 (2007) [arXiv:hep-ph/0607059].

[35] E. Aliu *et al.* [K2K Collaboration], Phys. Rev. Lett. **94**, 081802 (2005) [arXiv:hep-ex/0411038]; T. Araki *et al.* [KamLAND Collaboration], Phys. Rev. Lett. **94**, 081801 (2005) [arXiv:hep-ex/0406035].

[36] J. L. Feng, S. Su and F. Takayama, Phys. Rev. D **70**, 075019 (2004) [arXiv:hep-ph/0404231].

[37] D. N. Spergel *et al.* [WMAP Collaboration], Astrophys. J. Suppl. **170**, 377 (2007) [arXiv:astro-ph/0603449].

[38] J. F. Navarro, C. S. Frenk and S. D. M. White, Astrophys. J. **490**, 493 (1997) [arXiv:astro-ph/9611107].

[39] C. H. Chen, C. Q. Geng and D. V. Zhuridov, arXiv:0905.0652 [hep-ph].

[40] A. Ibarra and D. Tran, JCAP **0807**, 002 (2008) [arXiv:0804.4596 [astro-ph]].

[41] E. A. Baltz and J. Edsjo, Phys. Rev. D **59**, 023511 (1998) [arXiv:astro-ph/9808243].

[42] L. Zhang, X. Chen, M. Kamionkowski, Z. g. Si and Z. Zheng, Phys. Rev. D **76**, 061301 (2007) [arXiv:0704.2444 [astro-ph]].

[43] D. A. Demir and L. L. Everett, Phys. Rev. D **69**, 015008 (2004) [arXiv:hep-ph/0306240].

[44] A. Bottino, F. Donato, N. Fornengo and P. Salati, Phys. Rev. D **72**, 083518 (2005) [arXiv:hep-ph/0507086].